**THE EUROPEAN
PHYSICAL JOURNAL C**

Release note: VBFNLO 3.0

Julien Baglio[1]**, Francisco Campanario**[2]**, Tinghua Chen**[3]**, Heiko Dietrich-Siebert**[4]**, Terrance Figy**[5]**,
Matthias Kerner**[4]**, Michael Kubocz**[6]**, Duc Ninh Le**[7]**, Maximilian Löschner**[8]**, Simon Plätzer**[9,10]**, Michael Rauch**[4]**,
Ivan Rosario**[2,a] **, Robin Roth**[4]**, Dieter Zeppenfeld**[4]

[1] QuantumBasel, Schorenweg 44B, 4144 Arlesheim, Switzerland
[2] Theory Division, IFIC, University of Valencia-CSIC, Parque Científico, C/Catedrático José Beltrán, 2, 46980 Paterna, Spain
[3] IT Research Cyberinfrastructure, University of Delaware Newark, Newark, DE 19716, USA
[4] Institute for Theoretical Physics, Karlsruhe Institute of Technology (KIT), 76128 Karlsruhe, Germany
[5] Department of Mathematics, Statistics and Physics, Wichita State University, 1845 Fairmount Street, Wichita, KS 67067, USA
[6] Institut für Theoretische Teilchenphysik und Kosmologie, RWTH Aachen University, 52056 Aachen, Germany
[7] Phenikaa Institute for Advanced Study, Phenikaa University, Hanoi 12116, Vietnam
[8] Deutsches Elektronen-Synchrotron DESY, Notkestr. 85, 22607 Hamburg, Germany
[9] Institute of Physics, NAWI Graz, University of Graz, Universitätsplatz 5, 8010 Graz, Austria
[10] Particle Physics, Faculty of Physics, University of Vienna, Boltzmanngasse 5, 1090 Wien, Austria

Abstract VBFNLO is a flexible parton level Monte Carlo program for the simulation of vector boson fusion (VBF), QCD-induced single and double vector boson production plus two jets, and double and triple vector boson production (plus jet) in hadronic collisions at next-to-leading order (NLO) in the strong coupling constant, as well as Higgs boson plus two and three jet production via gluon fusion at the one-loop level. For the new version – VERSION 3.0 – several major enhancements have been included. An interface according to the Binoth Les Houches Accord (BLHA) has been added for all VBF and di/tri-boson processes including fully leptonic decays. For all dimension-8 operators affecting vector boson scattering (VBS) processes, a modified T-matrix unitarization procedure has been implemented. Several new production processes have been added, namely the VBS $Z\gamma jj$ and $\gamma\gamma jj$ processes at NLO, $\gamma\gamma jj$, WWj and ZZj production at NLO including the loop-induced gluon-fusion contributions and the gluon-fusion one-loop induced Φjjj (Φ is a CP-even or CP-odd scalar boson) process at LO, retaining the full top-mass dependence. Finally, the code has been parallelized using OPENMPI.

1 Introduction

The LHC has probed the Standard Model (SM) of particle physics to an unprecedented level of accuracy. After the dis-

covery of a narrow scalar resonance, with a mass around $m_H = 125$ GeV, compatible with the Higgs particle of the SM, and the lack of new heavier resonances, the beyond SM physics discovery potential of the LHC depends heavily on our ability to provide accurate cross-section predictions for both signal and background processes of multi-particle production processes involving jets, leptons, photons and missing energy.

A precise description of the hard, multi-particle production processes is needed, as well as a method for simulating the measurable hadronic final states. Furthermore, the flexibility to impose kinematic cuts is mandatory for processes involving QCD radiation, for example to reduce backgrounds or to account for the geometry of the detector. This makes analytic phase-space integration unfeasible and the implementation of results in the form of Monte Carlo programs becomes the method of choice.

Reaching these goals requires at least next-to-leading order (NLO) QCD calculations presented in the form of parton level Monte Carlo (MC) generators, which are an efficient solution when it comes to final states characterized by a high number of jets and/or identified particles.

To fully compare with the observed measurements, one needs parton shower event generators which properly account for the high final-state multiplicity due to QCD radiation, adding QCD emissions to fixed-order processes.

VBFNLO [1–3] is a flexible MC program for vector boson fusion (VBF) and vector boson scattering (VBS), QCD-induced single and double vector boson production plus

---

[a] e-mail: ivan.rosario@ific.uv.es (corresponding author)

Springer

two jets, and double and triple vector boson (plus jet) production processes at NLO QCD accuracy. Furthermore, the electroweak corrections to Higgs boson production via VBF (which are of the same order of magnitude as the QCD corrections in the experimentally accessible regions of phase-space) have been included. Since real emission processes are part of the NLO cross-sections, VBFNLO provides the means to calculate cross-sections for the corresponding process with one additional jet at leading order (LO) in the strong coupling.

VBFNLO can be run in the Minimal Supersymmetric Standard Model (MSSM), with real or complex parameters, for Higgs boson production via VBF. Anomalous couplings of the Higgs boson and electroweak gauge bosons have been implemented for a multitude of processes. Additionally, two Higgsless extra dimension models are included – the Warped Higgsless scenario and a Three-Site Higgsless Model – for selected processes. These models can be used to simulate the production of technicolor-type vector resonances in VBF and triple vector boson production. Diboson plus two jets production via VBF can also be run in a spin-2 model [4] and in a model with two Higgs resonances.

In addition, the simulation of CP-even and CP-odd Higgs boson production in gluon fusion, associated with up to three additional jets, is implemented at LO QCD. For these gluon fusion processes, the full top- and bottom-quark mass dependence of the one-loop contributions in the Standard Model (SM), in the MSSM and in a generic two-Higgs-doublet model is included.

Arbitrary cuts can be specified as well as various scale choices. Any currently available parton distribution function (PDF) set can be used through the LHAPDF library. In addition, a selected set of PDFs are hard-wired into the code (e.g. CT18 [5]). At leading order the program is capable of generating event files in the Les Houches Accord (LHA) and the HEPMC format, while for next-to-leading-order this can be done through the Binoth Les Houches Accord (BLHA) interface [6,7], for the processes where it is implemented. When working in the MSSM, the SUSY parameters can be input via a standard SLHA file.

In this article, we present the new version of the program VBFNLO, which includes as a major feature the creation of an interface at NLO according to the BLHA for all VBF and di/tri-boson processes including fully leptonic decays, which allows performing full simulations down to the particle level, if interfaced with a MC event generator, which will take care of parton shower and hadronization effects.

The VBFNLO program has been released via a series of versions 2.0, 2.5.0, 2.6.0, and 2.7.0. [1,2]. This version supersedes version 2.7.0, with the following new features:

- A BLHA interface for all VBS, double and triple vector boson production processes.
- Parallelization of the code with OPENMPI.

- The dimension 8 operator $\mathcal{O}_{S,2}$ has been added.
- For VBS, the K-matrix unitarization procedure has been implemented for the dimension 8 operator $\mathcal{O}_{S,1}$ and the isospin-conserving combination $\mathcal{O}_{S,0} \equiv \mathcal{O}_{S,2}$. For general dimension 8 operators, the so-called T_u model is implemented as an alternative unitarization procedure.
- Linking with LHAPDF v6 has been enabled.
- The following new processes have been added: WWj and ZZj production including the loop-induced gluon-fusion (GF) contributions of $\mathcal{O}(\alpha_s^3)$. QCD-induced $ZZjj$, VBS and QCD-induced $Z\gamma jj$ and $\gamma\gamma jj$, $Z(\to \ell^+\ell^-)Z(\to \nu\bar{\nu})\gamma$ production. The GF one-loop induced Φjjj process at LO, with $\Phi \in (h, A)$, with h and A general CP-even and CP-odd Higgs particles.
- Higgs decays have been implemented for the VBF-HHjj process.

Additionally, several bugfixes and smaller improvements have also been included. The complete list can be found in the CHANGELOG.md file included in the tarball.

1.1 Availability

The new program version, together with other useful tools and information, can be obtained from the webpage – https://ific.uv.es/vbfnlo/.

In order to improve our response to user queries, all problems and requests for user support should be reported via email to vbfnlo@ific.uv.es. VBFNLO is released under the GNU General Public License (GPL) version 2 and the MCnet guidelines for the distribution and usage of event generator software in an academic setting, which are distributed together with the source, and can also be obtained from http://www.montecarlonet.org.

1.2 Documentation and further details

The VBFNLO webpage – https://ific.uv.es/vbfnlo/ – contains, in addition to the updated manual, the previous versions of the program. Relevant publications and theses are also listed. Useful tools, such as for form factor calculation and for combining multiple independent runs (with different random seeds), are available under Downloads. A complete list of processes, with the utilities – BLHA interface, BSM models – currently available with them, can be found in Appendix A. More information about the BSM model implementations can be found in Appendix A in the VBFNLO manual.

1.3 Prerequisites

The basic installation requires GNU `make`, a FORTRAN 95[1] and a C++ compiler. VBFNLO offers the possibility of using the LHAPDF[2] [8] library (versions 5 and 6) for parton distribution functions. In order to include the electroweak corrections to VBF Higgs production, the program LOOPTOOLS[3] [9,10] is required. Additionally, FEYNHIGGS[4] [11–14] can be linked to the code in order to calculate the Higgs boson sector of the MSSM, although a SLHA file can be used as an alternative. If the simulation of Kaluza-Klein resonances is enabled, an installation of the GNU Scientific Library (GSL)[5] is required. VBFNLO can also be linked to ROOT[6] and HEPMC[7] to produce histograms and event files in those formats.

1.4 Installation and running the program

For detailed installation instructions and available compilation options, please refer to Chapter 2 of the VBFNLO Manual. The last version of the manual can be downloaded from `ific.uv.es/vbfnlo/downloads.html`. The Manual for the specific version of VBFNLO you downloaded can be found inside the `doc/` folder. The installation is performed in a standard UNIX-layout, i.e. the directory specified with the `--prefix` option of the `configure` script contains the following directories:

- `bin/`: vbfnlo executable.
- `include/VBFNLO/`: VBFNLO header files.
- `lib/VBFNLO/`: VBFNLO modules as dynamically loadable libraries. These can also be used independently from one of the main programs.
- `share/VBFNLO/`: Input files and internal PDF tables.

The vbfnlo executable contained in the `bin` directory of the installation path looks for the input files in the current working directory. Alternatively, the path to the input files can be specified explicitly by passing the `--input` argument to the program, e.g.

```
./bin/vbfnlo --input=[path to input
                files]
```

when running VBFNLO from the installation (`prefix`) directory. The input files contained in the `share/VBFNLO` directory are meant to represent default settings and should not be changed. We therefore recommend that the user copies the input files to a separate directory. Here, special settings may be chosen in the input files and the program can be run from that directory without specifying further options.

VBFNLO outputs a running 'log' to the terminal, containing information about the settings used and integrated cross-sections. In addition, a file (named `xsection.out`) is produced, which contains only the LO and NLO cross-sections, with the associated statistical errors. Additionally, histogram and event files can be output in various forms.

To enable a simple installation test, VBFNLO has a complete set of example results, together with input files, in the `regress` directory, which can be executed typing `make check`.

1.5 MPI, parallel jobs and optimised grids

MPI allows to run the VBFNLO code in parallel. Integration as well as grid and histogram generation are available with MPI parallelization, while for event output only single-core runs are supported.

To use it, first load OPENMPI in your environment (e.g. `module load openmpi`), then configure with `--enable-MPI` and the OpenMPI wrapper `FC=mpifort`.

To run the resulting binary start

```
mpirun -np 8 /prefix/bin/vbfnlo
```

replacing 8 with the number of requested parallel runs.

For single-core usage MPI and non-MPI runs should agree up to machine precision, while for multi-core runs, numerical differences up to the stated statistical uncertainty are expected.

Use the xoroshiro random number generator (`RTYPE=3` in `random.dat`) for best performance with MPI. For details see the manual, Sect. 5.9.

Owing to the complexity of the calculations involved, some of the processes implemented in VBFNLO (in particular the spin-2, triboson plus jet and QCD-induced diboson plus two jets processes) require a significant amount of time in order to obtain reasonable results. There are, however, methods which can be used in order to reduce the necessary run time or to further improve the statistics.

By using an optimised grid, the number of iterations needed in order to improve the efficiency of the MC integration can be reduced. This normally leads to a halving of the CPU time needed to achieve the same numerical accuracy. The optimised grids previously provided on the VBFNLO webpage are now no longer sustained, as they were tailored for a specific set of kinematic cuts and input parameters. They can be easily generated by the user (see the manual, Sects. 2.4.1 and 5.1.1, for instructions). A copy of the old set

---

[1] `gfortran` and `ifort` have been tested. Pure FORTRAN77 compilers like `g77` are no longer supported.

[2] https://lhapdf.hepforge.org/.

[3] http://www.feynarts.de/looptools/.

[4] http://www.feynhiggs.de/.

[5] https://www.gnu.org/software/gsl/.

[6] https://root.cern.ch/.

[7] http://lcgapp.cern.ch/project/simu/HepMC/.

of available grids can still be obtained in the Archive folder of the webpage.

Another method of improving the run time is to run several statistically independent jobs in parallel with or without MPI and then combine the results. In order to do this, several input directories need to be set up containing all the necessary `.dat` input files for the process. The variable `SEED` in `random.dat` (see the manual, Sect. 5.9) needs to be set to a different integer value in each directory. A short example of the results of a parallel run, together with their combination, is provided in the regress directory `regress/100_Hjj_parallel`. On the VBFNLO website, there is a shell script which can be used to combine the cross sections and histograms from parallel runs.

2 BLHA interface and usage with Herwig 7

An interface following the BLHA [6] and its update [7] (BLHA2) has been implemented in VBFNLO, and extensively tested with Herwig 7, for all di-boson, tri-boson and VBS processes with fully leptonic decays, the semi-leptonic decays are not yet included. This allows Herwig to use VBFNLO as a One-Loop Provider (OLP) through the Matchbox module [15]. The implemented interface only departs from the BLHA and BLHA2 in that it allows the use of the VBFNLO phase-space generator, which should increase the performance noticeably. Furthermore, instead of using SM matrix elements, VBFNLO can provide Herwig with matrix elements calculated using dim-6 and dim-8 operators in the Standard Model Effective Field Theory (SMEFT).

Herwig is able to perform NLO matching and merging using the matrix elements provided by VBFNLO. The MATCHBOX module [15] of Herwig includes two different matching procedures: a subtractive (MC@NLO-type) and a multiplicative (Powheg-type) NLO matching. Moreover, the implemented processes can be used for the (N)LO multi-jet merging outlined in Refs. [16,17]. Some phenomenological studies with the interfaced has been performed in Refs. [18–21].

If Herwig is installed using the `herwig-bootstrap` script, it will download and compile a copy of VBFNLO. The user can add the flag `--with-VBFNLO=PATH` during the run of the `herwig-boostrap` to use a local build of VBFNLO instead, where `PATH` is the path to the installation directory of the local VBFNLO.

If the user decides to use their own copy of VBFNLO and it is using a version of Herwig 7.3 or higher, they also have to add the `--enable-custom-blha` flag during the VBFNLO configuration. This modifies the standard BLHA interface to allow Herwig to call VBFNLO together with another OLP without name conflicts. Herwig 7.3 assumes this naming convention for VBFNLO 3.0 or higher. Trying to compile Herwig 7.3 with a VBFNLO 3.0 without this flag will result in a compilation error.

Curated input cards have been provided for the user in `VBFNLO/regress/runs/BLHA`. The user is advised to copy this input card as a starting template and modify it appropriately. Information about the different options can be found in the Herwig tutorial[8] and in Sect. 4 of the VBFNLO manual.

3 Unitarization and dimension-8 operators

Anomalous couplings can be described within an effective field theory (EFT) framework with operators of higher energy dimension ($d = 6, d = 8, \dots$)

$$\mathcal{L}_{\mathrm{EFT}} = \sum_i \frac{c_i^{(6)}}{\Lambda^2} \mathcal{O}_i^{(6)} + \sum_i \frac{c_i^{(8)}}{\Lambda^4} \mathcal{O}_i^{(8)} + \cdots . \tag{1}$$

Three new dimension-8 EFT operators have been implemented. The complete set can be found in Appendix A of the VBFNLO manual. Only bosonic operators are available in our program.

These higher dimensional operators can produce a violation of unitarity for some regions of phase-space, in particular for large center-of-mass energies of the scattering partons. This can be cured by using one of the unitarization procedures implemented in VBFNLO (form factors, K-matrix, and T_u-model, the latter two being available for VBS only). We highly suggest using the T_u-model for studying dimension-8 operators in VBS as it comes without the need for any additional ad hoc input parameters, which is an improvement over the form-factor method. Moreover, it not only cures unitarity violations at large center-of-mass energies of the scattering weak bosons, but also for large virtualities of the incoming vector bosons in VBS by suppressing the anomalous contribution sufficiently, which represents a major improvement over the K-matrix unitarization. It is also the only unitarization procedure in VBFNLO which works for the full set of dimension-8 operators that are implemented. For further details on the T_u-model and its implementation see Ref. [23].

4 New processes

4.1 New VBS and QCD-induced processes

Compared to the previous release note [3], several new VBS and QCD-induced processes have been implemented. The QCD-induced production of $ZZjj$ has been calculated in

---

Ref. [24], with the two Z boson system decaying either to four charged leptons, $ZZ \rightarrow l_1^+ l_1^- \, l_2^+ l_2^-$, or a pair of charged letons and a pair of neutrinos, $ZZ \rightarrow l^+ l^- \nu \bar{\nu}$. For the $Z\gamma jj$ channel, both the VBS as well as the QCD induced production have been implemented in Refs. [25,26] respectively, with the Z boson decaying to either a charged lepton pair or a pair of neutrinos. Similarly, the $\gamma\gamma jj$ production in the VBS and QCD channel have been implemented in Ref. [27]. Furthermore, the QCD-induced production of Zjj and γjj have been added to the program. The corresponding VBS production mechanisms have already been available in previous versions of VBFNLO.

The implementation of all processes follows a similar procedure. First, decay currents for the decays of the vector bosons $V \rightarrow l\bar{l}$ as well as $V \rightarrow l\bar{l}l'\bar{l}'$ are constructed, where the latter decay channel contains non-resonant contributions in the production of two vector bosons. For the VBS processes, in addition the leptonic tensors $V_1^\mu V_2^\nu \rightarrow l\bar{l}$ and $V_1^\mu V_2^\nu \rightarrow l\bar{l}l'\bar{l}'$ are constructed, which encode the scattering of the vector bosons V_i in the t- or u-channel. Here, $l\bar{l}$ and $l'\bar{l}'$ can either represent a charged lepton pair or a pair of neutrinos. For the $Z\gamma jj$ production processes, the code was adapted from the $ZZjj$ routine replacing the $l'\bar{l}'$ pair by the final-state photon. This procedure can be repeated to obtain the $\gamma\gamma jj$ code from the $Z\gamma jj$ one. The amplitudes of all partonic channels can then be obtained by contracting these currents with the quark lines involved in the process. Virtual corrections are obtained using the methods described in Ref. [28], grouping Feynman diagrams which only differ by permutations of the external currents into building blocks, leading to an efficient evaluation of these contributions. Gauge-invariance checks, where a current V^μ is replaced by its momentum, are used to guarantee the numerical stability of the code. A rescue system using quadruple precision is switched on when the gauge checks fail. This means that quadruple precision is used only for a fraction of statistics and, hence, does not appreciably affect the speed of the program. The virtual and real corrections are combined using the Catani-Seymour subtraction algorithm [29] to obtain infrared-finite NLO cross-sections. The final-state photon is treated using Frixione's smooth cone algorithm [30].

For all the new VBS $Z\gamma jj$ and $\gamma\gamma jj$ processes, anomalous gauge couplings are implemented using the effective Lagrangian with dimension-6 and 8 bosonic operators, see Sect. 3 for further details about these operators and available unitarization methods.

Extensive checks have been performed by comparing the tree-level and virtual amplitudes with the ones obtained by using automated tools such as Madgraph [31], FeynArts-3.4 [32], FormCalc-6.2 [9]. For the anomalous coupling part, we have cross-checked our implementation at the LO-amplitude level against Madgraph with the FeynRules [33,34] model file EWdim6 [35,36] (for dimension-6) and with the FeynRules model files for quartic-gauge couplings [37] (for dimension-8). Agreement at the machine-precision level has been found at random phase-space points.

4.2 Double vector boson production in association with a hadronic jet

The diboson plus jet processes $W^+W^- j$ and ZZj have been included at the NLO QCD level. As processes involving multiple electroweak bosons and jets, these are important channels in which to compare experimental data with the predictions of the Standard Model. The NLO QCD corrections to the total cross-sections are sizeable, and have a non-trivial phasespace dependence. As usual in the VBFNLO code, the leptonic decays of the vector bosons are included with all off-shell and spin correlation effects. These processes were included first as contributions to the approximate NNLO predictions of the WW and ZZ production processes presented in Refs. [38,39]. The technical implementation of the processes follows closely the procedure described in the previous sub-section. The implementation of the code has been tested at the amplitude and integrated cross-section level against Madgraph [31] for the LO and NLO-real corrections. As for the virtual corrections, internal checks based on factorization, gauge and reparametrization invariance, as described in Ref. [28], were implemented.

4.3 New gluon fusion induced processes

New Gluon Fusion (GF) processes have been implemented in comparison to the previous release note [3]. The one-loop induced WWj and ZZj gluon-fusion production processes have been included at LO. The ZZj channel was first computed for on-shell Z's in Ref. [40], where an extensive study of the stability of the code due to the presence of the Gram determinants was performed. A rescue system was implemented, using both standard tensor integrals reduction methods with quadruple precision and dedicated routines for small Gram determinants. This combination helped to reduce the impact of quadruple precision routines while minimizing numerical instabilities to an insignificant level.

The amplitudes are computed by building up a set of four master Feynman diagrams and attaching to them the corresponding particles, as described in detail in Ref. [40]. Afterwards, following the strategy presented in Sect. 4.1, the leptonic decays of the vector bosons, including all off-shell and spin correlation effects, were included. Both processes WWj and ZZj were also included as contributions to the higher order QCD corrections, $\mathcal{O}(\alpha_s^3)$, to the predictions of the WW and ZZ production processes presented in Refs. [38,39]. The full GF one-loop induced Φjjj process at LO has been included, with $\Phi \in (h, A)$, where h and A are general

CP-even and CP-odd Higgs particles, extending the results presented in Refs. [41,42], which only contained the purely gluonic channel. Finite bottom-mass loops have also been included since these corrections dominate in some BSM scenarios. Similar to the $GFVVj$ processes, the full amplitude is formed from a reduced set of Feynman master integrals, attaching to each of them the corresponding particles or currents to build a contributing Feynman diagram. The amplitudes have been cross-checked internally in the heavy-top limit, reaching a relative precision at the amplitude level of 10^{-5} or below for values of the top mass of 50 TeV.

Due to the numerically challenging one-loop times one-loop hexagon diagrams, a rescue system based on quadruple precision has been designed. Based on Ward identities to identify the instabilities, once an unstable diagram is identified, the scalar and tensor integrals are evaluated again in quadruple precision. If the point after this procedure is identified as stable, it is kept; otherwise, the complete amplitude is set to zero for the given phase space point. This procedure reduces the instabilities well below the per mille level while only mildly affecting the CPU time of the code.[9]

4.4 Higgs pair production in vector boson fusion including Higgs boson decays

Higgs pair production plus two jets via VBF is the second largest production channel at the LHC [43]. At leading order it is produced by electroweak quark-quark scattering processes, $qq' \rightarrow qq'HH$ and related crossings. The NLO QCD corrections in the VBF approximation are DIS-type QCD corrections to the scattering quark lines. The interference with the double Higgs-strahlung process $qq' \rightarrow V^* \rightarrow qq'HH$ is negligible, the latter process being viewed as an entirely separated production channel, see for example in Ref. [44].

The NLO QCD corrections correspond to virtual corrections to the $qq'V$ vertex as well as real emission contributions given by a gluon attached to a quark line, where either the gluon, the quark, or the anti-quark enter as the initial state particle. They were implemented following the strategy described in Sect. 4.1.

The decay of the Higgs boson pair in the final state can now also be included in VBFNLO. More specifically, given that the Higgs decay width is small, the narrow-width approximation provides accurate predictions for VBF production. The largest branching ratio in the SM is for $H \rightarrow b\bar{b}$. We have implemented the decay modes $pp \rightarrow qq'HH \rightarrow qq'b\bar{b}\gamma\gamma$ and $pp \rightarrow qq'HH \rightarrow qq'b\bar{b}\tau^+\tau^-$. The calculation uses the full $2 \rightarrow 6$ phase-space to define the kinematical quan-

tities. Note that the calculation can also be interfaced with Herwig as this is a VBF production mode, see Sect. 2 on how to interface VBFNLO and Herwig.

5 Other changes

The release VERSION 3.0 includes some changes that alter previous results:

5.1 NLO calculation of VBF-Hjj

Bugs have been removed in the virtual and real-emission parts of VBF-Hjj production, which leads to a decrease of the NLO cross-section of roughly 10%.

5.2 NLO calculation of VBF-$Z\gamma jj$ with anomalous couplings

A bug has been fixed in the real-emission part of VBF-$Z\gamma jj$ production when anomalous couplings were switched on.

5.3 NLO calculations of $W^- jj$, $W^- Zjj$, $W^- \gamma jj$ production

A bug in the PDF convolution of the QCD-induced production processes $W^- jj$, $W^- Zjj$ and $W^- \gamma jj$ has been fixed. The size of the effect, which can be observed both in the real-emission part of the NLO calculation and the corresponding LO+jet processes, can reach several percent, depending on the parameter settings.

5.4 VBF cuts for $HHjj$

VBF cuts now also apply to VBF production of a Higgs pair.

5.5 K-matrix unitarization

Following the introduction of the dimension 8 operator $\mathcal{O}_{S,2}$, the K-matrix unitarization procedure for $\mathcal{O}_{S,0}$ has been reworked. The relation to the parameters α_4 and α_5 of the electroweak chiral Lagrangian is now process-universal. To account for the isospin-conservation of these operators, which is used in the K-matrix procedure, only the combination $c_{S,0} = c_{S,2}$ can be unitarised, as well as $\mathcal{O}_{S,1}$. For other combinations the T_u-model can be used (see Sect. 3).

5.6 Calculation of histogram-bin errors

A bug has been found in the calculation of the statistical errors of histogram bins, which leads to an increase of the errors. The mean value of the cross-section (bin-wise) is unchanged.

---

[9] This process is disabled by default and must be enabled at compilation using the configure option – enable-processes=all or – enable-processes=ggf.

The statistical error of the integrated cross-section was correctly calculated, hence not affected by this change.

6 Example results

For illustration, we exhibit a small selection of differential distributions for the process $pp \rightarrow e^- \bar{\nu}_e jj + X$ through VBF at NLO QCD. These were computed in two different ways: using VBFNLO stand-alone and the VBFNLO-Herwig combination (denoted as Herwig here for short). Two different runs were perfomed using Herwig, namely a fixed order computation (Herwig FO), to check agreement with VBFNLO, and a parton shower matched with VBFNLO's amplitude (Herwig PS). The Herwig PS runs were done with the default angular ordered shower in Herwig matched with MC@NLO.

The runs are created at a center-of-mass energy of $\sqrt{s} = 13$ TeV in the 4-flavour scheme using fixed scales $\mu_F = \mu_R = 100$ GeV, and with the MMHT2014 PDFs [45], and

$$m_W = 80.377 \text{ GeV}, \quad \Gamma_W = 2.085 \text{ GeV},$$
$$m_Z = 91.1876 \text{ GeV}, \quad \Gamma_Z = 2.4952 \text{ GeV},$$
$$G_F = 1.16637 \cdot 10^{-5} \text{ GeV}^{-2}.$$

For the Herwig FO, both at the analysis and generation levels, and the VBFNLO runs, the following cuts are imposed: charged leptons are required to have

$$|y_e| < 2.5, \quad p_{T,e} > 20 \text{ GeV}, \tag{2}$$

while the jets are defined using the anti-k_T algorithm [46] with the radius parameter $R = 0.4$, and

$$|y_j| < 4.5, \quad p_{T,j} > 30 \text{ GeV}. \tag{3}$$

VBF cuts are also implemented with

$$\Delta y_{j_1 j_2} > 3.6, \quad m_{j_1 j_2} > 600 \text{ GeV}, \tag{4}$$

where j_1 and j_2 correspond to the two leading jets in p_T.

For the Herwig PS run, the generation level cuts were chosen to be as inclusive as possible: only requiring charged leptons to have

$$|y_e| < 5.0, \quad p_{T,e} > 10 \text{ GeV},$$

and not including any cut on jets. After events are generated, the analysis-level cuts Eqs. (2–4) are then applied to compute the kinematic distributions.

The resulting integrated cross-sections for the VBFNLO stand-alone run (labeled by VBFNLO) and for the Herwig FO
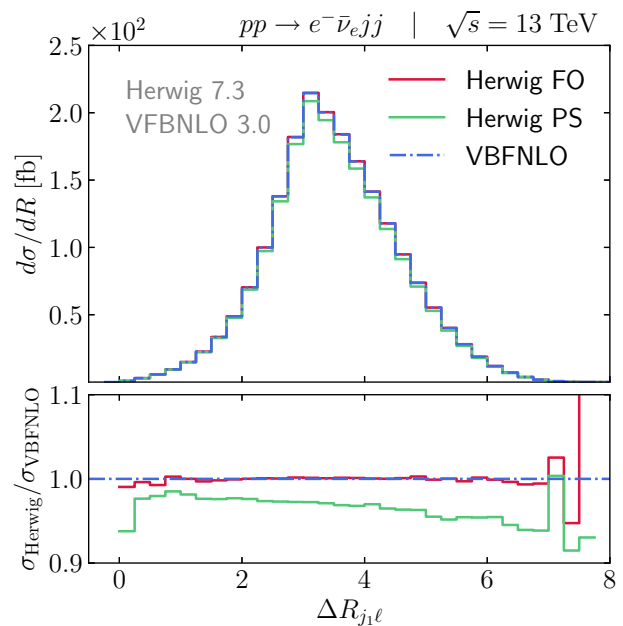

Fig. 1 R-separation between the hardest jet and the electron

run using VBFNLO as an OLP through the BLHA interface are

$$\sigma_{\text{VBFNLO}} = 496.64 \pm 0.03 \text{ fb} \tag{5}$$
$$\sigma_{\text{Herwig FO}} = 497.01 \pm 0.04 \text{ fb}. \tag{6}$$

The Herwig FO integrated cross-section was obtained from the analysis result of the fixed-order run.

In Figs. 1, 2, 3, we display distributions for the R-separation between the leading jet and the electron, the transverse momentum of the leading jet (the one with the highest p_T), and the transverse momentum of the neutrino, respectively, together with the ratios between Herwig and VBFNLO. The R-separation is defined as $R_{je} = \sqrt{(\phi_j - \phi_e)^2 + (y_j - y_e)^2}$, where ϕ_x is the azimuthal angle of particle x and y_x is the rapidity of particle x.

The distributions show a good agreement between the VBFNLO and the Herwig FO results while parton shower effects, for the current setup and selected distributions, stay at the few per cent level. These differences in the Herwig PS distributions are expected due to the additional QCD radiation effects by the parton shower, which are formally of higher order in α_s.

7 Summary and outlook

VBFNLO is a fully flexible partonic Monte Carlo program for vector boson fusion and scattering, as well as double and triple vector boson production processes at NLO QCD
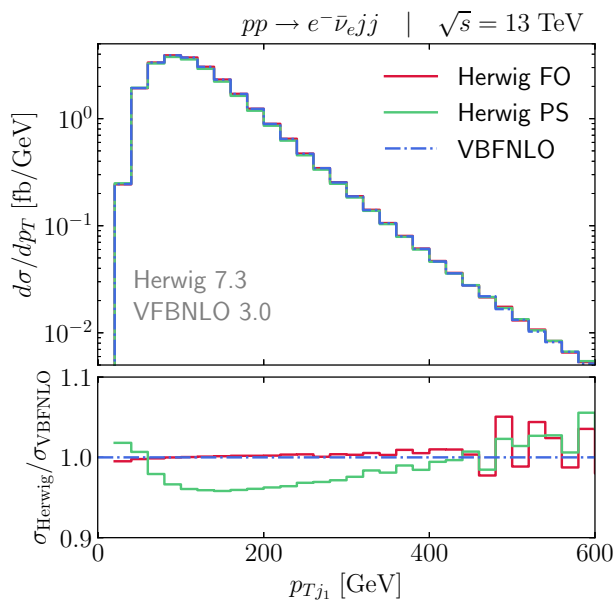
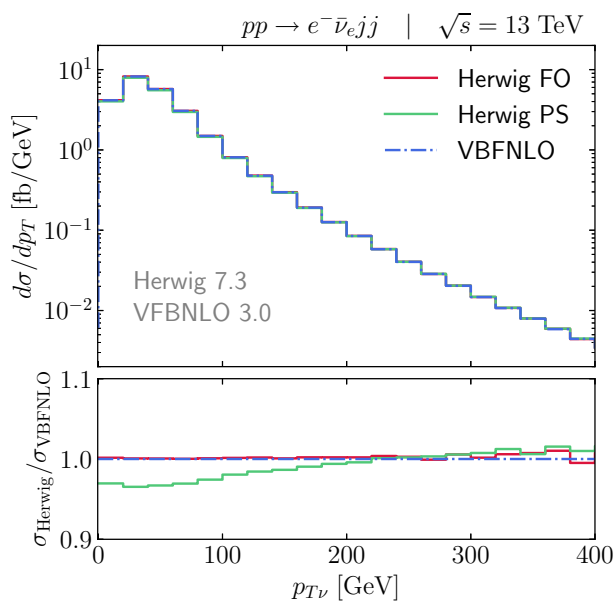**Fig. 2** Transverse momentum distribution of the hardest jet

Fig. 3 Transverse momentum distribution of the neutrino

and tested with the event generator Herwig and, second, the code has been parallelized using OpenMPI. Furthermore, additional features like new processes or unitarization procedures for dimension-8 operators in VBS processes, have been included.

Future improvements are directed along two main lines of development: Further processes at NLO QCD accuracy will be included and the BLHA interface will be extended to include other classes of processes.

Data Availability Statement This manuscript has no associated data. [Author's comment: Data sharing not applicable to this article as no datasets were generated or analysed during the current study.]

Code Availability Statement This manuscript has associated code/software in a data repository. [Author's comment: The source code is available in https://github.com/vbfnlo/vbfnlo. It also can be downloaded as a tarball from http://ific.uv.es/vbfnlo/.]

accuracy. The simulation of the one-loop CP-even and CP-odd Higgs boson production in gluon fusion, associated with two and three additional jets, is implemented at leading order, retaining the full top and bottom quark mass dependence.

In this release, two major features extend the usability of the program. First, a BLHA interface for all VBS, double and triple vector boson productions processes has been created

Appendix A: Process list

The following is a complete list of all processes available in VBFNLO, including any Beyond the Standard Model (BSM) effects that are implemented.

ProcId	Process	BLHA	Semi-leptonic decay	VBF process	Anom. gauge couplings	Anom. Higgs couplings	Two-Higgs model	Kaluza–Klein model	Spin-2 model	MSSM
100	$p \overset{(-)}{p} \to H\,jj$	✓	–	✓	–	✓	–	–	–	✓
101	$p \overset{(-)}{p} \to H\,jj \to \gamma\gamma\,jj$	–	–	✓	–	✓	–	–	–	✓
102	$p \overset{(-)}{p} \to H\,jj \to \mu^+\mu^-\,jj$	–	–	✓	–	✓	–	–	–	✓
103	$p \overset{(-)}{p} \to H\,jj \to \tau^+\tau^-\,jj$	–	–	✓	–	✓	–	–	–	✓
104	$p \overset{(-)}{p} \to H\,jj \to b\bar{b}\,jj$	–	–	✓	–	✓	–	–	–	✓
105	$p \overset{(-)}{p} \to H\,jj \to W^+W^-\,jj \to \ell_1^+\nu_{\ell_1}\ell_2^-\bar{\nu}_{\ell_2}\,jj$	–	–	✓	–	✓	–	–	–	✓
106	$p \overset{(-)}{p} \to H\,jj \to ZZ\,jj \to \ell_1^+\ell_1^-\ell_2^+\ell_2^-\,jj$	–	–	✓	–	✓	–	–	–	✓
107	$p \overset{(-)}{p} \to H\,jj \to ZZ\,jj \to \ell_1^+\ell_1^-\nu_{\ell_2}\bar{\nu}_{\ell_2}\,jj$	–	–	✓	–	✓	–	–	–	✓
108	$p \overset{(-)}{p} \to H\,jj \to W^+W^-\,jj \to q\bar{q}\,\ell^-\bar{\nu}_\ell\,jj$	–	✓	✓	–	✓	–	–	–	✓
109	$p \overset{(-)}{p} \to H\,jj \to W^+W^-\,jj \to \ell^+\nu_\ell\,q\bar{q}\,jj$	–	✓	✓	–	✓	–	–	–	✓
1010	$p \overset{(-)}{p} \to H\,jj \to ZZ\,jj \to q\bar{q}\,\ell^+\ell^-\,jj$	–	✓	✓	–	✓	–	–	–	✓
110	$p \overset{(-)}{p} \to H\,jjj$	–	–	✓	–	–	–	–	–	–
111	$p \overset{(-)}{p} \to H\,jjj \to \gamma\gamma\,jjj$	–	–	✓	–	–	–	–	–	–
112	$p \overset{(-)}{p} \to H\,jjj \to \mu^+\mu^-\,jjj$	–	–	✓	–	–	–	–	–	–
113	$p \overset{(-)}{p} \to H\,jjj \to \tau^+\tau^-\,jjj$	–	–	✓	–	–	–	–	–	–
114	$p \overset{(-)}{p} \to H\,jjj \to b\bar{b}\,jjj$	–	–	✓	–	–	–	–	–	–
115	$p \overset{(-)}{p} \to H\,jjj \to W^+W^-\,jjj \to \ell_1^+\nu_{\ell_1}\ell_2^-\bar{\nu}_{\ell_2}\,jjj$	–	–	✓	–	–	–	–	–	–
116	$p \overset{(-)}{p} \to H\,jjj \to ZZ\,jjj \to \ell_1^+\ell_1^-\ell_2^+\ell_2^-\,jjj$	–	–	✓	–	–	–	–	–	–
117	$p \overset{(-)}{p} \to H\,jjj \to ZZ\,jjj \to \ell_1^+\ell_1^-\nu_{\ell_2}\bar{\nu}_{\ell_2}\,jjj$	–	–	✓	–	–	–	–	–	–
120	$p \overset{(-)}{p} \to Z\,jj \to \ell^+\ell^-\,jj$	✓	–	✓	✓	–	–	–	–	–

PROCID	PROCESS	BLHA	Semi-leptonic decay	VBF process	Anom. gauge couplings	Anom. Higgs couplings	Two-Higgs model	Kaluza–Klein model	Spin-2 model	MSSM
121	$p\overset{(-)}{p} \to Z\,jj \to \nu_\ell \bar\nu_\ell\,jj$	✓	–	✓	✓	–	–	–	–	–
130	$p\overset{(-)}{p} \to W^+\,jj \to \ell^+\nu_\ell\,jj$	✓	–	✓	✓	–	–	–	–	–
140	$p\overset{(-)}{p} \to W^-\,jj \to \ell^-\bar\nu_\ell\,jj$	✓	–	✓	✓	–	–	–	–	–
150	$p\overset{(-)}{p} \to \gamma\,jj$	✓	–	✓	✓	–	–	–	–	–
191	$p\overset{(-)}{p} \to S_2\,jj \to \gamma\gamma\,jj$	–	–	✓	–	–	–	–	✓	–
195	$p\overset{(-)}{p} \to S_2\,jj \to W^+W^-\,jj \to \ell_1^+\nu_{\ell_1}\ell_2^-\bar\nu_{\ell_2}\,jj$	–	–	✓	–	–	–	–	✓	–
196	$p\overset{(-)}{p} \to S_2\,jj \to ZZ\,jj \to \ell_1^+\ell_1^-\ell_2^+\ell_2^-\,jj$	–	–	✓	–	–	–	–	✓	–
197	$p\overset{(-)}{p} \to S_2\,jj \to ZZ\,jj \to \ell_1^+\ell_1^-\nu_{\ell_2}\bar\nu_{\ell_2}\,jj$	–	–	✓	–	–	–	–	✓	–
160	$p\overset{(-)}{p} \to HH\,jj$	–	–	✓	–	–	–	–	–	–
161	$p\overset{(-)}{p} \to HH\,jj \to b\bar b\tau^+\tau^-\,jj$	–	–	✓	–	–	–	–	–	–
162	$p\overset{(-)}{p} \to HH\,jj \to b\bar b\gamma\gamma\,jj$	–	–	✓	–	–	–	–	–	–
2100	$p\overset{(-)}{p} \to H\gamma\,jj$	–	–	✓	–	–	–	–	–	–
2101	$p\overset{(-)}{p} \to H\gamma\,jj \to \gamma\gamma\gamma\,jj$	–	–	✓	–	–	–	–	–	–
2102	$p\overset{(-)}{p} \to H\gamma\,jj \to \mu^+\mu^-\gamma\,jj$	–	–	✓	–	–	–	–	–	–
2103	$p\overset{(-)}{p} \to H\gamma\,jj \to \tau^+\tau^-\gamma\,jj$	–	–	✓	–	–	–	–	–	–
2104	$p\overset{(-)}{p} \to H\gamma\,jj \to b\bar b\gamma\,jj$	–	–	✓	–	–	–	–	–	–
2105	$p\overset{(-)}{p} \to H\gamma\,jj \to W^+W^-\gamma\,jj \to \ell_1^+\nu_{\ell_1}\ell_2^-\bar\nu_{\ell_2}\gamma\,jj$	–	–	✓	–	–	–	–	–	–
2106	$p\overset{(-)}{p} \to H\gamma\,jj \to ZZ\gamma\,jj \to \ell_1^+\ell_1^-\ell_2^+\ell_2^-\gamma\,jj$	–	–	✓	–	–	–	–	–	–
2107	$p\overset{(-)}{p} \to H\gamma\,jj \to ZZ\gamma\,jj \to \ell_1^+\ell_1^-\nu_{\ell_2}\bar\nu_{\ell_2}\gamma\,jj$	–	–	✓	–	–	–	–	–	–
200	$p\overset{(-)}{p} \to W^+W^-\,jj \to \ell_1^+\nu_{\ell_1}\ell_2^-\bar\nu_{\ell_2}\,jj$	✓	–	✓	✓	–	✓	✓	✓	–
201	$p\overset{(-)}{p} \to W^+W^-\,jj \to q\bar q\,\ell^-\bar\nu_\ell\,jj$	–	✓	✓	✓	–	✓	–	–	–

PROCID	PROCESS	BLHA	Semi-leptonic decay	VBF process	Anom. gauge couplings	Anom. Higgs couplings	Two-Higgs model	Kaluza–Klein model	Spin-2 model	MSSM
202	$p\overset{(-)}{p} \to W^+W^- jj \to \ell^+\nu_\ell\, q\bar{q}\, jj$	–	✓	✓	✓	–	✓	–	–	–
210	$p\overset{(-)}{p} \to ZZ\, jj \to \ell_1^+\ell_1^-\ell_2^+\ell_2^-\, jj$	✓	–	✓	✓	–	✓	✓	✓	–
211	$p\overset{(-)}{p} \to ZZ\, jj \to \ell_1^+\ell_1^-\nu_{\ell_2}\bar{\nu}_{\ell_2}\, jj$	✓	–	✓	✓	–	✓	✓	✓	–
212	$p\overset{(-)}{p} \to ZZ\, jj \to q\bar{q}\,\ell^+\ell^-\, jj$	–	✓	✓	✓	–	✓	–	–	–
220	$p\overset{(-)}{p} \to W^+Z\, jj \to \ell_1^+\nu_{\ell_1}\ell_2^+\ell_2^-\, jj$	✓	–	✓	✓	–	✓	✓	✓	–
221	$p\overset{(-)}{p} \to W^+Z\, jj \to q\bar{q}\,\ell^+\ell^-\, jj$	–	✓	✓	✓	–	✓	–	–	–
222	$p\overset{(-)}{p} \to W^+Z\, jj \to \ell^+\nu_\ell\, q\bar{q}\, jj$	–	✓	✓	✓	–	✓	–	–	–
230	$p\overset{(-)}{p} \to W^-Z\, jj \to \ell_1^-\bar{\nu}_{\ell_1}\ell_2^+\ell_2^-\, jj$	✓	–	✓	✓	–	✓	✓	✓	–
231	$p\overset{(-)}{p} \to W^-Z\, jj \to q\bar{q}\,\ell^+\ell^-\, jj$	–	✓	✓	✓	–	✓	–	–	–
232	$p\overset{(-)}{p} \to W^-Z\, jj \to \ell^-\bar{\nu}_\ell\, q\bar{q}\, jj$	–	✓	✓	✓	–	✓	–	–	–
240	$p\overset{(-)}{p} \to \gamma\gamma\, jj$	✓	–	✓	✓	–	–	–	–	–
250	$p\overset{(-)}{p} \to W^+W^+ jj \to \ell_1^+\nu_{\ell_1}\ell_2^+\nu_{\ell_2}\, jj$	✓	–	✓	✓	–	✓	–	–	–
251	$p\overset{(-)}{p} \to W^+W^+ jj \to q\bar{q}\,\ell^+\nu_\ell\, jj$	–	✓	✓	✓	–	✓	–	–	–
260	$p\overset{(-)}{p} \to W^-W^- jj \to \ell_1^-\bar{\nu}_{\ell_1}\ell_2^-\bar{\nu}_{\ell_2}\, jj$	✓	–	✓	✓	–	✓	–	–	–
261	$p\overset{(-)}{p} \to W^-W^- jj \to q\bar{q}\,\ell^-\bar{\nu}_\ell\, jj$	–	✓	✓	✓	–	✓	–	–	–
270	$p\overset{(-)}{p} \to W^+\gamma\, jj \to \ell^+\nu_\ell\gamma\, jj$	✓	–	✓	✓	–	–	–	–	–

PROCID	PROCESS	BLHA	Semi-leptonic decay	VBF process	Anom. gauge couplings	Anom. Higgs couplings	Two-Higgs model	Kaluza–Klein model	Spin-2 model	MSSM
280	$p \overset{(-)}{p} \to W^- \gamma\, jj \to \ell^- \bar{\nu}_\ell \gamma\, jj$	✓	–	✓	✓	–	–	–	–	–
290	$p \overset{(-)}{p} \to Z\gamma\, jj \to \ell^+ \ell^- \gamma\, jj$	✓	–	✓	✓	–	–	–	–	–
291	$p \overset{(-)}{p} \to Z\gamma\, jj \to \nu_\ell \bar{\nu}_\ell \gamma\, jj$	✓	–	✓	✓	–	–	–	–	–
3120	$p \overset{(-)}{p} \to Z\, jj \to \ell^+ \ell^-\, jj$	–	–	–	–	–	–	–	–	–
3121	$p \overset{(-)}{p} \to Z\, jj \to \nu_\ell \bar{\nu}_\ell\, jj$	–	–	–	–	–	–	–	–	–
3130	$p \overset{(-)}{p} \to W^+\, jj \to \ell^+ \nu_\ell\, jj$	–	–	–	–	–	–	–	–	–
3140	$p \overset{(-)}{p} \to W^-\, jj \to \ell^- \bar{\nu}_\ell\, jj$	–	–	–	–	–	–	–	–	–
3210	$p \overset{(-)}{p} \to ZZ\, jj \to \ell_1^+ \ell_1^- \ell_2^+ \ell_2^-\, jj$	–	–	–	–	–	–	–	–	–
3211	$p \overset{(-)}{p} \to ZZ\, jj \to \ell_1^+ \ell_1^- \nu_{\ell_2} \bar{\nu}_{\ell_2}\, jj$	–	–	–	–	–	–	–	–	–
3220	$p \overset{(-)}{p} \to W^+ Z\, jj \to \ell_1^+ \nu_{\ell_1} \ell_2^+ \ell_2^-\, jj$	–	–	–	–	–	–	–	–	–
3230	$p \overset{(-)}{p} \to W^- Z\, jj \to \ell_1^- \bar{\nu}_{\ell_1} \ell_2^+ \ell_2^-\, jj$	–	–	–	–	–	–	–	–	–
3240	$p \overset{(-)}{p} \to \gamma\gamma\, jj$	–	–	–	–	–	–	–	–	–
3250	$p \overset{(-)}{p} \to W^+ W^+\, jj \to \ell_1^+ \nu_{\ell_1} \ell_2^+ \nu_{\ell_2}\, jj$	–	–	–	–	–	–	–	–	–
3260	$p \overset{(-)}{p} \to W^- W^-\, jj \to \ell_1^- \bar{\nu}_{\ell_1} \ell_2^- \bar{\nu}_{\ell_2}\, jj$	–	–	–	–	–	–	–	–	–
3270	$p \overset{(-)}{p} \to W^+ \gamma\, jj \to \ell^+ \nu_\ell \gamma\, jj$	–	–	–	–	–	–	–	–	–

PROCID	PROCESS	BLHA	Semi-leptonic decay	VBF process	Anom. gauge couplings	Anom. Higgs couplings	Two-Higgs model	Kaluza–Klein model	Spin-2 model	MSSM
3280	$p \overset{(-)}{p} \to W^- \gamma\, jj \to \ell^- \bar{\nu}_\ell \gamma\, jj$	–	–	–	–	–	–	–	–	–
3290	$p \overset{(-)}{p} \to Z \gamma\, jj \to \ell^+ \ell^- \gamma\, jj$	–	–	–	–	–	–	–	–	–
3291	$p \overset{(-)}{p} \to Z \gamma\, jj \to \nu_\ell \bar{\nu}_\ell \gamma\, jj$	–	–	–	–	–	–	–	–	–
1330	$p \overset{(-)}{p} \to W^+ \to \ell^+ \nu_\ell$	–	–	–	–	–	–	–	–	–
1340	$p \overset{(-)}{p} \to W^- \to \ell^- \bar{\nu}_\ell$	–	–	–	–	–	–	–	–	–
1630	$p \overset{(-)}{p} \to W^+ j \to \ell^+ \nu_\ell\, j$	–	–	–	–	–	–	–	–	–
1640	$p \overset{(-)}{p} \to W^- j \to \ell^- \bar{\nu}_\ell\, j$	–	–	–	–	–	–	–	–	–
300	$p \overset{(-)}{p} \to W^+ W^- \to \ell_1^+ \nu_{\ell_1} \ell_2^- \bar{\nu}_{\ell_2}$	✓	–	–	✓	✓	–	–	–	–
301	$p \overset{(-)}{p} \to W^+ W^- \to q\bar{q}\, \ell^- \bar{\nu}_\ell$	–	✓	–	✓	✓	–	–	–	–
302	$p \overset{(-)}{p} \to W^+ W^- \to \ell^+ \nu_\ell\, q\bar{q}$	–	✓	–	✓	✓	–	–	–	–
310	$p \overset{(-)}{p} \to W^+ Z \to \ell_1^+ \nu_{\ell_1} \ell_2^+ \ell_2^-$	✓	–	–	✓	–	–	–	–	–
312	$p \overset{(-)}{p} \to W^+ Z \to q\bar{q}\, \ell^+ \ell^-$	–	✓	–	✓	–	–	–	–	–
313	$p \overset{(-)}{p} \to W^+ Z \to \ell^+ \nu_\ell\, q\bar{q}$	–	✓	–	✓	–	–	–	–	–
320	$p \overset{(-)}{p} \to W^- Z \to \ell_1^- \bar{\nu}_{\ell_1} \ell_2^+ \ell_2^-$	✓	–	–	✓	–	–	–	–	–
322	$p \overset{(-)}{p} \to W^- Z \to q\bar{q}\, \ell^+ \ell^-$	–	✓	–	✓	–	–	–	–	–
323	$p \overset{(-)}{p} \to W^- Z \to \ell^- \bar{\nu}_\ell\, q\bar{q}$	–	✓	–	✓	–	–	–	–	–

PROCID	PROCESS	BLHA	Semi-leptonic decay	VBF process	Anom. gauge couplings	Anom. Higgs couplings	Two-Higgs model	Kaluza–Klein model	Spin-2 model	MSSM
330	$p \overset{(-)}{p} \to ZZ \to \ell_1^- \ell_1^+ \ell_2^- \ell_2^+$	✓	–	–	–	✓	–	–	–	–
331	$p \overset{(-)}{p} \to ZZ \to q\bar{q}\,\ell^- \ell^+$	–	✓	–	–	✓	–	–	–	–
340	$p \overset{(-)}{p} \to W^+\gamma \to \ell_1^+ \nu_{\ell_1} \gamma$	✓	–	–	✓	–	–	–	–	–
350	$p \overset{(-)}{p} \to W^-\gamma \to \ell_1^- \bar{\nu}_{\ell_1} \gamma$	✓	–	–	✓	–	–	–	–	–
360	$p \overset{(-)}{p} \to Z\gamma \to \ell_1^- \ell_1^+ \gamma$	✓	–	–	–	✓	–	–	–	–
370	$p \overset{(-)}{p} \to \gamma\gamma$	✓	–	–	–	✓	–	–	–	–
1300	$p \overset{(-)}{p} \to W^+ H \to \ell^+ \nu_\ell H$	–	–	–	✓	–	–	–	–	–
1301	$p \overset{(-)}{p} \to W^+ H \to \ell^+ \nu_\ell \gamma\gamma$	–	–	–	✓	–	–	–	–	–
1302	$p \overset{(-)}{p} \to W^+ H \to \ell^+ \nu_\ell \mu^+\mu^-$	–	–	–	✓	–	–	–	–	–
1303	$p \overset{(-)}{p} \to W^+ H \to \ell^+ \nu_\ell \tau^+\tau^-$	–	–	–	✓	–	–	–	–	–
1304	$p \overset{(-)}{p} \to W^+ H \to \ell^+ \nu_\ell b\bar{b}$	–	–	–	✓	–	–	–	–	–
1305	$p \overset{(-)}{p} \to W^+ H \to W^+W^+W^- \to \ell_1^+ \nu_{\ell_1} \ell_2^+ \nu_{\ell_2} \ell_3^- \bar{\nu}_{\ell_3}$	–	–	–	✓	–	–	–	–	–
1306	$p \overset{(-)}{p} \to W^+ H \to W^+ZZ \to \ell_1^+ \nu_{\ell_1} \ell_2^+ \ell_2^- \ell_3^+ \ell_3^-$	–	–	–	✓	–	–	–	–	–
1307	$p \overset{(-)}{p} \to W^+ H \to W^+ZZ \to \ell_1^+ \nu_{\ell_1} \ell_2^+ \ell_2^- \nu_{\ell_3} \bar{\nu}_{\ell_3}$	–	–	–	✓	–	–	–	–	–
1310	$p \overset{(-)}{p} \to W^- H \to \ell^- \bar{\nu}_\ell H$	–	–	–	✓	–	–	–	–	–
1311	$p \overset{(-)}{p} \to W^- H \to \ell^- \bar{\nu}_\ell \gamma\gamma$	–	–	–	✓	–	–	–	–	–
1312	$p \overset{(-)}{p} \to W^- H \to \ell^- \bar{\nu}_\ell \mu^+\mu^-$	–	–	–	✓	–	–	–	–	–
1313	$p \overset{(-)}{p} \to W^- H \to \ell^- \bar{\nu}_\ell \tau^+\tau^-$	–	–	–	✓	–	–	–	–	–
1314	$p \overset{(-)}{p} \to W^- H \to \ell^- \bar{\nu}_\ell b\bar{b}$	–	–	–	✓	–	–	–	–	–

PROCID	PROCESS	BLHA	semi-leptonic decay	VBF process	anom. gauge couplings	anom. Higgs couplings	Two-Higgs model	Kaluza-Klein model	Spin-2 model	MSSM
1315	$p \overset{(-)}{p} \to W^- H \to W^- W^+ W^- \to \ell_1^- \bar{\nu}_{\ell_1} \ell_2^+ \nu_{\ell_2} \ell_3^- \bar{\nu}_{\ell_3}$	–	–	–	✓	–	–	–	–	–
1316	$p \overset{(-)}{p} \to W^- H \to W^- Z Z \to \ell_1^- \bar{\nu}_{\ell_1} \ell_2^+ \ell_2^- \ell_3^+ \ell_3^-$	–	–	–	✓	–	–	–	–	–
1317	$p \overset{(-)}{p} \to W^- H \to W^- Z Z \to \ell_1^- \bar{\nu}_{\ell_1} \ell_2^+ \ell_2^- \nu_{\ell_3} \bar{\nu}_{\ell_3}$	–	–	–	✓	–	–	–	–	–
600	$p \overset{(-)}{p} \to W^+ W^- j \to \ell_1^+ \nu_{\ell_1} \ell_2^- \bar{\nu}_{\ell_2} j$	–	–	–	–	✓	–	–	–	–
601	$p \overset{(-)}{p} \to W^+ W^- j \to q \bar{q} \ell^- \bar{\nu}_\ell j$	–	✓	–	–	–	–	–	–	–
602	$p \overset{(-)}{p} \to W^+ W^- j \to \ell^+ \nu_\ell q \bar{q} j$	–	✓	–	–	–	–	–	–	–
610	$p \overset{(-)}{p} \to W^- \gamma j \to \ell^- \bar{\nu}_\ell \gamma j$	–	–	–	✓	–	–	–	–	–
620	$p \overset{(-)}{p} \to W^+ \gamma j \to \ell^+ \nu_\ell \gamma j$	–	–	–	✓	–	–	–	–	–
630	$p \overset{(-)}{p} \to W^- Z j \to \ell_1^- \bar{\nu}_{\ell_1} \ell_2^- \ell_2^+ j$	–	–	–	✓	–	–	–	–	–
640	$p \overset{(-)}{p} \to W^+ Z j \to \ell_1^+ \nu_{\ell_1} \ell_2^- \ell_2^+ j$	–	–	–	✓	–	–	–	–	–
650	$p \overset{(-)}{p} \to Z Z j \to \ell_1^+ \ell_1^- \ell_2^+ \ell_2^- j$	–	–	–	–	✓	–	–	–	–
1600	$p \overset{(-)}{p} \to W^+ H j \to \ell^+ \nu_\ell H j$	–	–	–	✓	–	–	–	–	–
1601	$p \overset{(-)}{p} \to W^+ H j \to \ell^+ \nu_\ell \gamma \gamma j$	–	–	–	✓	–	–	–	–	–
1602	$p \overset{(-)}{p} \to W^+ H j \to \ell^+ \nu_\ell \mu^+ \mu^- j$	–	–	–	✓	–	–	–	–	–

PROCID	PROCESS	BLHA	Semi-leptonic decay	VBF process	Anom. gauge couplings	Anom. Higgs couplings	Two-Higgs model	Kaluza–Klein model	Spin-2 model	MSSM
1603	$p \overset{(-)}{p} \to W^+ H j \to \ell^+ \nu_\ell \tau^+ \tau^- j$	–	–	–	✓	–	–	–	–	–
1604	$p \overset{(-)}{p} \to W^+ H j \to \ell^+ \nu_\ell b \bar{b} j$	–	–	–	✓	–	–	–	–	–
1605	$p \overset{(-)}{p} \to W^+ H j \to W^+ W^+ W^- j \to \ell_1^+ \nu_{\ell_1} \ell_2^+ \nu_{\ell_2} \ell_3^- \bar{\nu}_{\ell_3} j$	–	–	–	✓	–	–	–	–	–
1606	$p \overset{(-)}{p} \to W^+ H j \to W^+ Z Z j \to \ell_1^+ \nu_{\ell_1} \ell_2^+ \ell_2^- \ell_3^+ \ell_3^- j$	–	–	–	✓	–	–	–	–	–
1607	$p \overset{(-)}{p} \to W^+ H j \to W^+ Z Z j \to \ell_1^+ \nu_{\ell_1} \ell_2^+ \ell_2^- \nu_{\ell_3} \bar{\nu}_{\ell_3} j$	–	–	–	✓	–	–	–	–	–
1610	$p \overset{(-)}{p} \to W^- H j \to \ell^- \bar{\nu}_\ell H j$	–	–	–	✓	–	–	–	–	–
1611	$p \overset{(-)}{p} \to W^- H j \to \ell^- \bar{\nu}_\ell \gamma \gamma j$	–	–	–	✓	–	–	–	–	–
1612	$p \overset{(-)}{p} \to W^- H j \to \ell^- \bar{\nu}_\ell \mu^+ \mu^- j$	–	–	–	✓	–	–	–	–	–
1613	$p \overset{(-)}{p} \to W^- H j \to \ell^- \bar{\nu}_\ell \tau^+ \tau^- j$	–	–	–	✓	–	–	–	–	–
1614	$p \overset{(-)}{p} \to W^- H j \to \ell^- \bar{\nu}_\ell b \bar{b} j$	–	–	–	✓	–	–	–	–	–
1615	$p \overset{(-)}{p} \to W^- H j \to W^- W^+ W^- j \to \ell_1^- \bar{\nu}_{\ell_1} \ell_2^+ \nu_{\ell_2} \ell_3^- \bar{\nu}_{\ell_3} j$	–	–	–	✓	–	–	–	–	–
1616	$p \overset{(-)}{p} \to W^- H j \to W^- Z Z j \to \ell_1^- \bar{\nu}_{\ell_1} \ell_2^+ \ell_2^- \ell_3^+ \ell_3^- j$	–	–	–	✓	–	–	–	–	–
1617	$p \overset{(-)}{p} \to W^- H j \to W^- Z Z j \to \ell_1^- \bar{\nu}_{\ell_1} \ell_2^+ \ell_2^- \nu_{\ell_3} \bar{\nu}_{\ell_3} j$	–	–	–	✓	–	–	–	–	–

ProcId	Process	BLHA	Semi-leptonic decay	VBF process	Anom. gauge couplings	Anom. Higgs couplings	Two-Higgs model	Kaluza–Klein model	Spin-2 model	MSSM
400	$p \overset{(-)}{p} \rightarrow W^+W^-Z \rightarrow \ell_1^+ \nu_{\ell_1} \ell_2^- \bar{\nu}_{\ell_2} \ell_3^+ \ell_3^-$	✓	–	–	✓	–	–	✓	–	–
401	$p \overset{(-)}{p} \rightarrow W^+W^-Z \rightarrow q\bar{q} \, \ell_1^- \bar{\nu}_{\ell_1} \ell_2^+ \ell_2^-$	–	✓	–	✓	–	–	–	–	–
402	$p \overset{(-)}{p} \rightarrow W^+W^-Z \rightarrow \ell_1^+ \nu_{\ell_1} q\bar{q} \, \ell_2^+ \ell_2^-$	–	✓	–	✓	–	–	–	–	–
403	$p \overset{(-)}{p} \rightarrow W^+W^-Z \rightarrow \ell_1^+ \nu_{\ell_1} \ell_2^- \bar{\nu}_{\ell_2} q\bar{q}$	–	✓	–	✓	–	–	–	–	–
410	$p \overset{(-)}{p} \rightarrow ZZW^+ \rightarrow \ell_1^+ \ell_1^- \ell_2^+ \ell_2^- \ell_3^+ \nu_{\ell_3}$	✓	–	–	✓	–	–	✓	–	–
411	$p \overset{(-)}{p} \rightarrow ZZW^+ \rightarrow \ell_1^+ \ell_1^- \ell_2^+ \ell_2^- q\bar{q}$	–	✓	–	✓	–	–	–	–	–
412	$p \overset{(-)}{p} \rightarrow ZZW^+ \rightarrow q\bar{q} \, \ell_1^+ \ell_1^- \ell_2^+ \nu_{\ell_2}$	–	✓	–	✓	–	–	–	–	–
420	$p \overset{(-)}{p} \rightarrow ZZW^- \rightarrow \ell_1^+ \ell_1^- \ell_2^+ \ell_2^- \ell_3^- \bar{\nu}_{\ell_3}$	✓	–	–	✓	–	–	✓	–	–
421	$p \overset{(-)}{p} \rightarrow ZZW^- \rightarrow \ell_1^+ \ell_1^- \ell_2^+ \ell_2^- q\bar{q}$	–	✓	–	✓	–	–	–	–	–
422	$p \overset{(-)}{p} \rightarrow ZZW^- \rightarrow q\bar{q} \, \ell_1^+ \ell_1^- \ell_2^- \bar{\nu}_{\ell_2}$	–	✓	–	✓	–	–	–	–	–
430	$p \overset{(-)}{p} \rightarrow W^+W^-W^+ \rightarrow \ell_1^+ \nu_{\ell_1} \ell_2^- \bar{\nu}_{\ell_2} \ell_3^+ \nu_{\ell_3}$	✓	–	–	✓	–	–	✓	–	–
431	$p \overset{(-)}{p} \rightarrow W^+W^-W^+ \rightarrow q\bar{q} \, \ell_1^- \bar{\nu}_{\ell_1} \ell_2^+ \nu_{\ell_2}$	–	✓	–	✓	–	–	–	–	–
432	$p \overset{(-)}{p} \rightarrow W^+W^-W^+ \rightarrow \ell_1^+ \nu_{\ell_1} q\bar{q} \, \ell_2^+ \nu_{\ell_2}$	–	✓	–	✓	–	–	–	–	–
440	$p \overset{(-)}{p} \rightarrow W^-W^+W^- \rightarrow \ell_1^- \bar{\nu}_{\ell_1} \ell_2^+ \nu_{\ell_2} \ell_3^- \bar{\nu}_{\ell_3}$	✓	–	–	✓	–	–	✓	–	–
441	$p \overset{(-)}{p} \rightarrow W^-W^+W^- \rightarrow \ell_1^- \bar{\nu}_{\ell_1} q\bar{q} \, \ell_2^- \bar{\nu}_{\ell_2}$	–	✓	–	✓	–	–	–	–	–
442	$p \overset{(-)}{p} \rightarrow W^-W^+W^- \rightarrow q\bar{q} \, \ell_1^+ \nu_{\ell_1} \ell_2^- \bar{\nu}_{\ell_2}$	–	✓	–	✓	–	–	–	–	–
450	$p \overset{(-)}{p} \rightarrow ZZZ \rightarrow \ell_1^- \ell_1^+ \ell_2^- \ell_2^+ \ell_3^- \ell_3^+$	✓	–	–	✓	–	–	–	–	–
451	$p \overset{(-)}{p} \rightarrow ZZZ \rightarrow q\bar{q} \, \ell_1^- \ell_1^+ \ell_2^- \ell_2^+$	–	✓	–	✓	–	–	–	–	–
460	$p \overset{(-)}{p} \rightarrow W^-W^+\gamma \rightarrow \ell_1^- \bar{\nu}_{\ell_1} \ell_2^+ \nu_{\ell_2} \gamma$	✓	–	–	✓	–	–	–	–	–

PROCID	PROCESS	BLHA	Semi-leptonic decay	VBF process	Anom. gauge couplings	Anom. Higgs couplings	Two-Higgs model	Kaluza–Klein model	Spin-2 model	MSSM
461	$p\,\overset{(-)}{p} \to W^+W^-\gamma \to q\bar{q}\,\ell^-\bar{\nu}_\ell\gamma$	–	✓	–	✓	–	–	–	–	–
462	$p\,\overset{(-)}{p} \to W^+W^-\gamma \to \ell^+\nu_\ell\,q\bar{q}\,\gamma$	–	✓	–	✓	–	–	–	–	–
470	$p\,\overset{(-)}{p} \to ZZ\gamma \to \ell_1^-\ell_1^+\ell_2^-\ell_2^+\gamma$	✓	–	–	✓	–	–	–	–	–
471	$p\,\overset{(-)}{p} \to ZZ\gamma \to \ell^-\ell^+\,q\bar{q}\,\gamma$	–	✓	–	✓	–	–	–	–	–
472	$p\,\overset{(-)}{p} \to ZZ\gamma \to \ell_1^-\ell_1^+\nu_{\ell_2}\bar{\nu}_{\ell_2}\gamma$	✓	–	–	–	–	–	–	–	–
480	$p\,\overset{(-)}{p} \to W^+Z\gamma \to \ell_1^+\nu_{\ell_1}\ell_2^-\ell_2^+\gamma$	✓	–	–	✓	–	–	–	–	–
481	$p\,\overset{(-)}{p} \to W^+Z\gamma \to q\bar{q}\,\ell^-\ell^+\gamma$	–	✓	–	✓	–	–	–	–	–
482	$p\,\overset{(-)}{p} \to W^+Z\gamma \to \ell^+\nu_\ell\,q\bar{q}\,\gamma$	–	✓	–	✓	–	–	–	–	–
490	$p\,\overset{(-)}{p} \to W^-Z\gamma \to \ell_1^-\bar{\nu}_{\ell_1}\ell_2^-\ell_2^+\gamma$	✓	–	–	✓	–	–	–	–	–
491	$p\,\overset{(-)}{p} \to W^-Z\gamma \to q\bar{q}\,\ell^-\ell^+\gamma$	–	✓	–	✓	–	–	–	–	–
492	$p\,\overset{(-)}{p} \to W^-Z\gamma \to \ell^-\bar{\nu}_\ell\,q\bar{q}\,\gamma$	–	✓	–	✓	–	–	–	–	–
500	$p\,\overset{(-)}{p} \to W^+\gamma\gamma \to \ell^+\nu_\ell\gamma\gamma$	✓	–	–	✓	–	–	–	–	–
510	$p\,\overset{(-)}{p} \to W^-\gamma\gamma \to \ell^-\bar{\nu}_\ell\gamma\gamma$	✓	–	–	✓	–	–	–	–	–
520	$p\,\overset{(-)}{p} \to Z\gamma\gamma \to \ell^-\ell^+\gamma\gamma$	✓	–	–	✓	–	–	–	–	–
521	$p\,\overset{(-)}{p} \to Z\gamma\gamma \to \nu_\ell\bar{\nu}_\ell\gamma\gamma$	✓	–	–	✓	–	–	–	–	–
530	$p\,\overset{(-)}{p} \to \gamma\gamma\gamma$	✓	–	–	–	–	–	–	–	–
800	$p\,\overset{(-)}{p} \to W^+\gamma\gamma j \to \ell^+\nu_\ell\gamma\gamma j$	–	–	–	✓	–	–	–	–	–
810	$p\,\overset{(-)}{p} \to W^-\gamma\gamma j \to \ell^-\bar{\nu}_\ell\gamma\gamma j$	–	–	–	✓	–	–	–	–	–

The gluon-fusion processes are given below.

PROCID	PROCESS	BLHA	Gluon-fusion process	Semi-leptonic decay	Anom. Higgs couplings	Deneral 2HDM	MSSM
4100	$p\overset{(-)}{p} \to H\,jj$	–	✓	–	–	✓	✓
4101	$p\overset{(-)}{p} \to H\,jj \to \gamma\gamma\,jj$	–	✓	–	–	–	✓
4102	$p\overset{(-)}{p} \to H\,jj \to \mu^+\mu^-\,jj$	–	✓	–	–	–	✓
4103	$p\overset{(-)}{p} \to H\,jj \to \tau^+\tau^-\,jj$	–	✓	–	–	–	✓
4104	$p\overset{(-)}{p} \to H\,jj \to b\bar{b}\,jj$	–	✓	–	–	–	✓
4105	$p\overset{(-)}{p} \to H\,jj \to W^+W^-\,jj \to \ell_1^+\nu_{\ell_1}\ell_2^-\bar\nu_{\ell_2}\,jj$	–	✓	–	✓	✓	✓
4106	$p\overset{(-)}{p} \to H\,jj \to ZZ\,jj \to \ell_1^+\ell_1^-\ell_2^+\ell_2^-\,jj$	–	✓	–	✓	✓	✓
4107	$p\overset{(-)}{p} \to H\,jj \to ZZ\,jj \to \ell_1^+\ell_1^-\nu_{\ell_2}\bar\nu_{\ell_2}\,jj$	–	✓	–	✓	✓	✓
4200	$p\overset{(-)}{p} \to H\,jjj$	–	✓	–	–	✓	✓
4300	$p\overset{(-)}{p} \to W^+W^- \to \ell_1^+\nu_{\ell_1}\ell_2^-\bar\nu_{\ell_2}$	–	✓	–	✓	–	–
4301	$p\overset{(-)}{p} \to W^+W^- \to q\bar{q}\,\ell^-\bar\nu_\ell$	–	✓	✓	✓	–	–
4302	$p\overset{(-)}{p} \to W^+W^- \to \ell^+\nu_\ell\,q\bar{q}$	–	✓	✓	✓	–	–
4330	$p\overset{(-)}{p} \to ZZ \to \ell_1^-\ell_1^+\ell_2^-\ell_2^+$	–	✓	–	✓	–	–
4331	$p\overset{(-)}{p} \to ZZ \to q\bar{q}\,\ell^-\ell^+$	–	✓	✓	✓	–	–
4360	$p\overset{(-)}{p} \to Z\gamma \to \ell_1^-\ell_1^+\gamma$	–	✓	–	✓	–	–
4370	$p\overset{(-)}{p} \to \gamma\gamma$	–	✓	–	✓	–	–
4600	$p\overset{(-)}{p} \to W^+W^-j \to \ell_1^+\nu_{\ell_1}\ell_2^-\bar\nu_{\ell_2}j$	–	✓	–	✓	–	–
4601	$p\overset{(-)}{p} \to W^+W^-j \to q\bar{q}\,\ell^-\bar\nu_\ell\,j$	–	✓	✓	–	–	–
4602	$p\overset{(-)}{p} \to W^+W^-j \to \ell^+\nu_\ell q\bar{q}\,j$	–	✓	✓	–	–	–
4650	$p\overset{(-)}{p} \to ZZj \to \ell_1^-\ell_1^+\ell_2^-\ell_2^+j$	–	✓	–	✓	–	–

References

1. K. Arnold et al., VBFNLO: a parton level Monte Carlo for processes with electroweak bosons. Comput. Phys. Commun. Ser. **180**, 1661 (2009). https://doi.org/10.1016/j.cpc.2009.03.006. arXiv:0811.4559

2. J. Baglio et al., VBFNLO: a parton level Monte Carlo for processes with electroweak bosons—manual for version 2.7.0. arXiv:1107.4038

3. J. Baglio et al., Release note—VBFNLO 2.7.0. arXiv:1404.3940

4. J. Frank, M. Rauch, D. Zeppenfeld, Spin-2 resonances in vector-boson-fusion processes at next-to-leading order QCD. Phys. Rev. D Ser. **87**, 055020 (2013). https://doi.org/10.1103/PhysRevD.87.055020. arXiv:1211.3658

5. T.-J. Hou et al., New CTEQ global analysis of quantum chromodynamics with high-precision data from the LHC. Phys. Rev. D Ser. **103**, 014013 (2021). https://doi.org/10.1103/PhysRevD.103.014013. arXiv:1912.10053

6. T. Binoth et al., A proposal for a standard interface between Monte Carlo tools and one-loop programs. Comput. Phys. Commun. Ser. **181**, 1612 (2010). https://doi.org/10.1016/j.cpc.2010.05.016. arXiv:1001.1307

7. S. Alioli et al., Update of the Binoth Les Houches Accord for a standard interface between Monte Carlo tools and one-loop programs. Comput. Phys. Commun. Ser. **185**, 560 (2014). https://doi.org/10.1016/j.cpc.2013.10.020. arXiv:1308.3462

8. M.R. Whalley, D. Bourilkov, R.C. Group, The Les Houches accord PDFs (LHAPDF) and LHAGLUE, in *HERA and the LHC: A Workshop on the Implications of HERA and LHC Physics (Startup Meeting, CERN, 26–27 March 2004; Midterm Meeting, CERN, 11–13 October 2004)* (2005), pp. 575–581, 8. arXiv:hep-ph/0508110

9. T. Hahn, M. Perez-Victoria, Automatized one loop calculations in four-dimensions and D-dimensions. Comput. Phys. Commun. Ser. **118**, 153 (1999). https://doi.org/10.1016/S0010-4655(98)00173-8. arXiv:hep-ph/9807565

10. T. Hahn, M. Rauch, News from FormCalc and LoopTools. Nucl. Phys. B Proc. Suppl. Ser. **157**, 236 (2006). https://doi.org/10.1016/j.nuclphysbps.2006.03.026. arXiv:hep-ph/0601248

11. M. Frank, T. Hahn, S. Heinemeyer, W. Hollik, H. Rzehak, G. Weiglein, The Higgs boson masses and mixings of the complex MSSM in the Feynman-diagrammatic approach. JHEP Ser. **02**, 047 (2007). https://doi.org/10.1088/1126-6708/2007/02/047. arXiv:hep-ph/0611326

12. G. Degrassi, S. Heinemeyer, W. Hollik, P. Slavich, G. Weiglein, Towards high precision predictions for the MSSM Higgs sector. Eur. Phys. J. C Ser. **28**, 133 (2003). https://doi.org/10.1140/epjc/s2003-01152-2. arXiv:hep-ph/0212020

13. S. Heinemeyer, W. Hollik, G. Weiglein, The masses of the neutral CP—even Higgs bosons in the MSSM: accurate analysis at the two loop level. Eur. Phys. J. C Ser. **9**, 343 (1999). https://doi.org/10.1007/s100529900006. arXiv:hep-ph/9812472

14. S. Heinemeyer, W. Hollik, G. Weiglein, FeynHiggs: a program for the calculation of the masses of the neutral CP even Higgs bosons in the MSSM. Comput. Phys. Commun. Ser. **124**, 76 (2000). https://doi.org/10.1016/S0010-4655(99)00364-1. arXiv:hep-ph/9812320

15. S. Platzer, S. Gieseke, Dipole showers and automated NLO matching in Herwig++. Eur. Phys. J. C Ser. **72**, 2187 (2012). https://doi.org/10.1140/epjc/s10052-012-2187-7. arXiv:1109.6256

16. S. Plätzer, Controlling inclusive cross sections in parton shower + matrix element merging. JHEP Ser. **08**, 114 (2013). https://doi.org/10.1007/JHEP08(2013)114. arXiv:1211.5467

17. J. Bellm, S. Gieseke, S. Plätzer, Merging NLO multi-jet calculations with improved unitarization. Eur. Phys. J. C Ser. **78**, 244 (2018). https://doi.org/10.1140/epjc/s10052-018-5723-2. arXiv:1705.06700

18. M. Rauch, S. Plätzer, Parton shower matching systematics in Vector-Boson-Fusion WW production. Eur. Phys. J. C **77**, 293 (2017). arXiv:1605.07851

19. T. Chen, Anomalous Higgs boson couplings in vector boson fusion, Ph.D. thesis, Wichita State U (2023)

20. T. Chen, T.M. Figy, S. Plätzer, NLO multijet merging for Higgs production beyond the VBF approximation. Eur. Phys. J. C **82**, 704 (2022). arXiv:2109.03730

21. C. Bittrich, P. Kirchgaeßer, A. Papaefstathiou, S. Plätzer, S. Todt, Soft QCD effects in VBS/VBF topologies. Eur. Phys. J. C **82**, 783 (2022). arXiv:2110.01623

22. F. Campanario, T.M. Figy, S. Plätzer, M. Rauch, P. Schichtel, M. Sjödahl, Stress testing the vector-boson-fusion approximation in multijet final states. Phys. Rev. D **98**, 033003 (2018). arXiv:1802.09955

23. G. Perez, M. Sekulla, D. Zeppenfeld, Anomalous quartic gauge couplings and unitarization for the vector boson scattering process $pp \rightarrow W^+W^+jjX \rightarrow \ell^+\nu_\ell \ell^+\nu_\ell jjX$. Eur. Phys. J. C Ser. **78**, 759 (2018). https://doi.org/10.1140/epjc/s10052-018-6230-1. arXiv:1807.02707

24. F. Campanario, M. Kerner, L.D. Ninh, D. Zeppenfeld, Next-to-leading order QCD corrections to ZZ production in association with two jets. JHEP Ser. **07**, 148 (2014). https://doi.org/10.1007/JHEP07(2014)148. arXiv:1405.3972

25. F. Campanario, M. Kerner, D. Zeppenfeld, $Z\gamma$ production in vector-boson scattering at next-to-leading order QCD. JHEP Ser. **01**, 160 (2018). https://doi.org/10.1007/JHEP01(2018)160. arXiv:1704.01921

26. F. Campanario, M. Kerner, L.D. Ninh, D. Zeppenfeld, $Z\gamma$ production in association with two jets at next-to-leading order QCD. Eur. Phys. J. C Ser. **74**, 3085 (2014). https://doi.org/10.1140/epjc/s10052-014-3085-y. arXiv:1407.7857

27. F. Campanario, M. Kerner, N.D. Le, I. Rosario, Diphoton production in vector-boson scattering at the LHC at next-to-leading order QCD. JHEP Ser. **06**, 072 (2020). https://doi.org/10.1007/JHEP06(2020)072. arXiv:2002.12109

28. F. Campanario, Towards $pp \rightarrow VVjj$ at NLO QCD: bosonic contributions to triple vector boson production plus jet. JHEP Ser. **10**, 070 (2011). https://doi.org/10.1007/JHEP10(2011)070. arXiv:1105.0920

29. S. Catani, M.H. Seymour, A general algorithm for calculating jet cross-sections in NLO QCD. Nucl. Phys. B Ser. **485**, 291 (1997). https://doi.org/10.1016/S0550-3213(96)00589-5. arXiv:hep-ph/9605323

30. S. Frixione, Isolated photons in perturbative QCD. Phys. Lett. B Ser. **429**, 369 (1998). https://doi.org/10.1016/S0370-2693(98)00454-7. arXiv:hep-ph/9801442

31. J. Alwall, P. Demin, S. de Visscher, R. Frederix, M. Herquet, F. Maltoni et al., MadGraph/MadEvent v4: the new web generation. JHEP Ser. **09**, 028 (2007). https://doi.org/10.1088/1126-6708/2007/09/028. arXiv:0706.2334

32. T. Hahn, Generating Feynman diagrams and amplitudes with FeynArts 3. Comput. Phys. Commun. Ser. **140**, 418 (2001). https://doi.org/10.1016/S0010-4655(01)00290-9. arXiv:hep-ph/0012260

33. N.D. Christensen, C. Duhr, FeynRules—Feynman rules made easy. Comput. Phys. Commun. Ser. **180**, 1614 (2009). https://doi.org/10.1016/j.cpc.2009.02.018. arXiv:0806.4194

34. N.D. Christensen, P. de Aquino, C. Degrande, C. Duhr, B. Fuks, M. Herquet et al., A comprehensive approach to new physics simulations. Eur. Phys. J. C Ser. **71**, 1541 (2011). https://doi.org/10.1140/epjc/s10052-011-1541-5. arXiv:0906.2474

35. C. Degrande, O. Eboli, B. Feigl, B. Jäger, W. Kilian, O. Mattelaer et al., Monte Carlo tools for studies of non-standard electroweak gauge boson interactions in multi-boson processes: a snowmass white paper. (2013). arXiv:1309.7890

36. C. Degrande, N. Greiner, W. Kilian, O. Mattelaer, H. Mebane, T. Stelzer et al., Effective field theory: a modern approach to anomalous couplings. Ann. Phys. Ser. **335**, 21 (2013). https://doi.org/10.1016/j.aop.2013.04.016. arXiv:1205.4231

37. O.J.P. Eboli, M.C. Gonzalez-Garcia, J.K. Mizukoshi, $pp \rightarrow jje^{\pm}\mu^{\pm}\nu\nu$ and $jje^{\pm}\mu^{\mp}\nu\nu$ at $\mathcal{O}(\alpha_{em}^{6})$ and $\mathcal{O}(\alpha_{em}^{4}\alpha_{s}^{2})$ for the study of the quartic electroweak gauge boson vertex at CERN LHC. Phys. Rev. Ser. **D74**, 073005 (2006). https://doi.org/10.1103/PhysRevD.74.073005. arXiv:hep-ph/0606118

38. F. Campanario, M. Rauch, S. Sapeta, $W^{+}W^{-}$ production at high transverse momenta beyond NLO. Nucl. Phys. B Ser. **879**, 65 (2014). https://doi.org/10.1016/j.nuclphysb.2013.12.001. arXiv:1309.7293

39. F. Campanario, M. Rauch, S. Sapeta, ZZ production at high transverse momenta beyond NLO QCD. JHEP Ser. **08**, 070 (2015). https://doi.org/10.1007/JHEP08(2015)070. arXiv:1504.05588

40. F. Campanario, Q. Li, M. Rauch, M. Spira, ZZ+jet production via gluon fusion at the LHC. JHEP Ser. **06**, 069 (2013). https://doi.org/10.1007/JHEP06(2013)069. arXiv:1211.5429

41. F. Campanario, M. Kubocz, Higgs boson production in association with three jets via gluon fusion at the LHC: gluonic contributions. Phys. Rev. D Ser. **88**, 054021 (2013). https://doi.org/10.1103/PhysRevD.88.054021. arXiv:1306.1830

42. F. Campanario, M. Kubocz, Higgs boson CP-properties of the gluonic contributions in Higgs plus three jet production via gluon fusion at the LHC. JHEP Ser. **10**, 173 (2014). https://doi.org/10.1007/JHEP10(2014)173. arXiv:1402.1154

43. J. Alison et al., Higgs boson potential at colliders: status and perspectives. Rev. Phys. Ser. **5**, 100045 (2020). https://doi.org/10.1016/j.revip.2020.100045. arXiv:1910.00012

44. J. Baglio, A. Djouadi, R. Gröber, M.M. Mühlleitner, J. Quevillon, M. Spira, The measurement of the Higgs self-coupling at the LHC: theoretical status. JHEP Ser. **04**, 151 (2013). https://doi.org/10.1007/JHEP04(2013)151. arXiv:1212.5581

45. L.A. Harland-Lang, A.D. Martin, P. Motylinski, R.S. Thorne, Parton distributions in the LHC era: MMHT 2014 PDFs. Eur. Phys. J. C Ser. **75**, 204 (2015). https://doi.org/10.1140/epjc/s10052-015-3397-6. arXiv:1412.3989

46. M. Cacciari, G.P. Salam, G. Soyez, The anti-k_t jet clustering algorithm. JHEP Ser. **04**, 063 (2008). https://doi.org/10.1088/1126-6708/2008/04/063. arXiv:0802.1189